Piezoelectric MEMS Flexural-Plate-Wave Transducer for Alignment of Microparticles in a Drying Droplet

Alessandro Nastro, *Member, IEEE*, Marco Baù, *Member, IEEE*, Marco Ferrari, *Member, IEEE*, Libor Rufer, *Senior Member, IEEE*, Skandar Basrour, *Member, IEEE*, and Vittorio Ferrari, *Senior Member, IEEE*

***Abstract*—The possibility of obtaining aligned clusters of microparticles in a drying water droplet by employing standing flexural plate waves (FPWs) generated by a piezoelectric MEMS transducer has been explored. The MEMS device has a squared cavity etched out in a silicon (Si) substrate forming a 6 × 6 mm diaphragm composed of a stack of doped Si and aluminum nitride (AlN) layers. Metal interdigital transducers (IDTs) placed at the edges of the diaphragm allow to electrically drive the AlN layer to excite FPWs in the diaphragm at its first antisymmetric Lamb mode (A_0). The working principle has been validated through finite-element analysis and experimentally verified. For experimental testing, a droplet of tap water with an approximate radius of 850 μm was placed on the diaphragm and let dry at room temperature while applying voltage excitations to two opposed IDTs. After droplet evaporation, dry clusters of microparticles, originally dispersed therein, have been successfully patterned with a regular spacing of half wavelength, as expected, and remained adhered to the diaphragm without the need for additional substances for clot creation. The innovative exploitation of a noncontact and noninvasive flow-field-based approach combined with the evaporation process in a piezoelectric MEMS transducer can enhance the assembly control of microparticles or biological cells in lab-on-chip applications.**

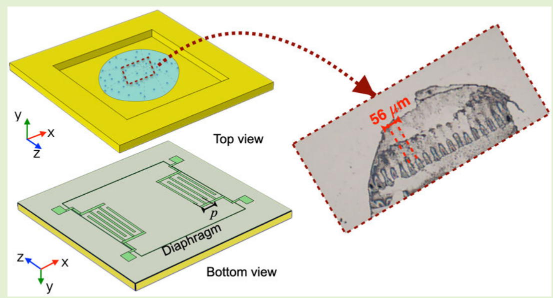

***Index Terms*—Acoustic waves, alignment, droplet evaporation, finite element method (FEM), flexural plate waves (FPWs), MEMS, microparticles assembly, piezoelectric, piezoelectric multiuser MEMS process (PiezoMUMPs), transducer.**

I. Introduction

THE capability to control the assembly of microscale objects has long been instrumental for tailoring the mechanical, optical, and electronic properties of materials. For instance, the assembly of G-wires [1] is of interest in the biomedical field since it can lead to the synthesis of four-stranded deoxyribonucleic acid (DNA) with enhanced optical and electronic properties, superior resistance to enzymatic degradation as well as mechanical and thermal stability on substrates [2]. The electrochemical, optical, and electromechanical properties of elongated particles such as carbon nanotubes can be enhanced by controlling the synthesis process along a preferred spatial direction [3]. Oriented assembly of single-crystalline TiO_2 nanorods on a transparent conductive substrate has allowed to successfully develop dye-sensitized solar cells [4]. Controlled assembly of microparticles has been effectively employed to build tailored bioactive membranes for drug delivery [5] and to develop platforms for cell analysis [6]. Microassembly approaches typically mimic nature by employing rather weak and specific interaction forces, which are essential to achieve the desired structures and functionalities. However, this requires a high degree of control to direct the aggregation and alignment processes [7]. Microparticle assembly can be typically achieved by relying on interparticle interactions or employing external stimuli and fields.

Chemical-based processes offer control through molecular interactions but have the drawback of being ineffective to

Manuscript received 29 December 2023; revised 18 January 2024; accepted 18 January 2024. Date of publication 26 January 2024; date of current version 14 March 2024. The associate editor coordinating the review of this article and approving it for publication was Dr. Wensong Wang. *(Corresponding author: Alessandro Nastro.)*

Alessandro Nastro, Marco Baù, Marco Ferrari, and Vittorio Ferrari are with the Department of Information Engineering, University of Brescia, 25123 Brescia, Italy (e-mail: alessandro.nastro@unibs.it; marco.bau@unibs.it; marco.ferrari@unibs.it; vittorio.ferrari@unibs.it).

Libor Rufer is with ADT MEMS, 38140 Grenoble, France (e-mail: libor.rufer@univ-grenoble-alpes.fr).

Skandar Basrour is with CNRS, Grenoble INP, TIMA, University Grenoble Alpes, 38000 Grenoble, France (e-mail: skandar.basrour@univ-grenoble-alpes.fr).

Digital Object Identifier 10.1109/JSEN.2024.3356708

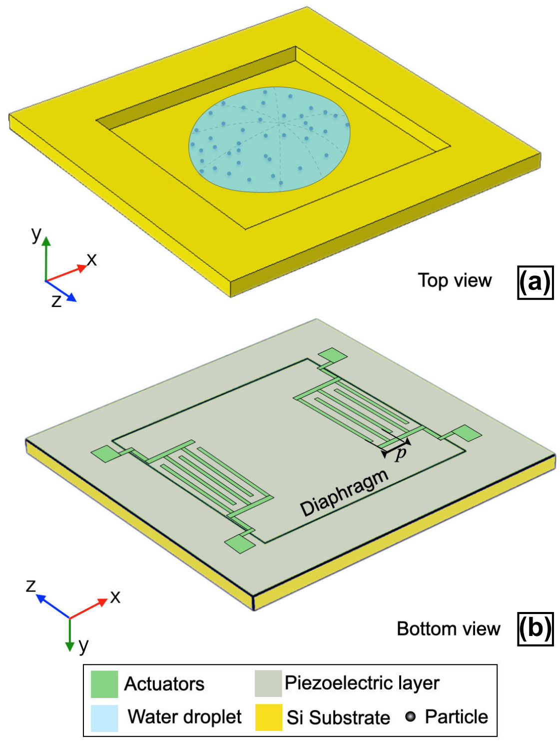

Fig. 1. (a) Top and (b) bottom schematic views of the proposed piezoelectric MEMS transducer.

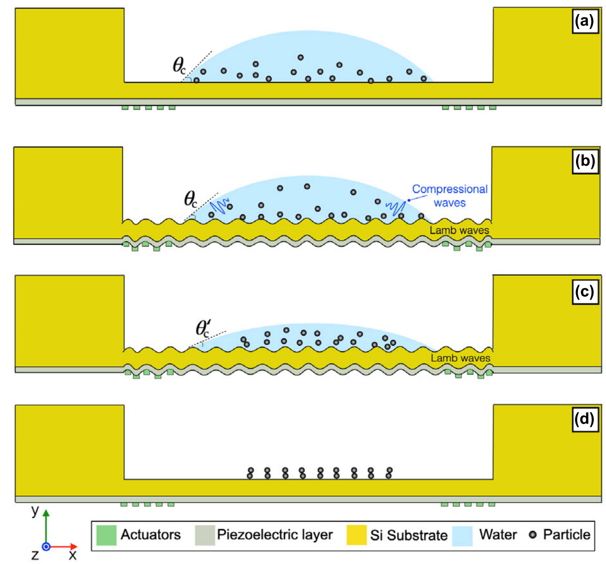

Fig. 2. Cross-sectional views of the proposed piezoelectric MEMS device illustrating the microparticle alignment process steps: (a) water droplet deposition; (b) electrical excitation; (c) evaporation; and (d) particle patterning.

cover large surface areas with respect to particle volume [8]. Electric-based processes leverage on the possibility to polarize microparticles with electric fields exploiting their dielectric properties that are mismatched with the surrounding medium [9], while magnetic-based processes manage to align and pattern particles relying on permanent magnetic dipoles [10].

However, both approaches have the disadvantage of not being fully compliant with biological applications since they can alter cell integrity, thus irreversibly damaging the biological tissue [11].

To achieve microassembly ensuring biocompatibility, flow-field approaches exploiting macroscopic viscous flows to direct the assembly of a disordered suspension of particles into ordered structures represent a valid alternative [12], [13]. Among flow-field techniques, acoustophoresis, i.e., the use of acoustic forces to act on particles and cells in microfluidic systems, has attracted interest to manipulate bioparticles due to its label-free noninvasive approach [14], [15]. Specifically, microfluidic systems based on acoustic waves generated through the piezoelectric effect have been largely adopted in biological and medical fields for mixing, separating, and aligning particles or cells [16], [17], [18]. Surface acoustic wave (SAW), bulk acoustic wave (BAW), and flexural plate wave (FPW) acoustic modes can be generated and detected by piezoelectric transducers [19], [20], [21], [22]. Compared with SAW and BAW, FPW-based devices typically exhibit, for a given wavelength, a lower excitation frequency in the range of 5–20 MHz, which reduces the demands on the driving electronics [23]. The acoustic waves are employed to interact with fluids, steer particles dispersed therein, and assemble microstructures at micrometric resolution [24]. A possible limitation in some applications is that, once the flow is removed, the created assembly can possibly revert into disordered particles unless additional substances are added to create clots [13]. To this purpose, an evaporation-based assembly process employing droplets deposited on surfaces can be an effective solution [25]. Droplets are used as vehicles to obtain patterned deposits of microparticles, which remain adhered to the surface after liquid evaporation [26]. Furthermore, the dynamics of the acousto-mechanical impedance of drying droplets in combination with the pattern left after liquid evaporation can be used as a diagnostic tool [27]. The use of an evaporation-based process with ultrasonic excitation has been employed to form a circular spot of silver nanowires (AgNWs) and to radially align AgNWs on the device surface [28]. Battery electrodes have been developed by exploiting a rapid evaporation of mixed solvents to enable directional ion transport via forming vertically aligned nanosheets [29]. In this context, this work explores the possibility to innovatively combine a non-contact and noninvasive flow-field-based approach with the label-free evaporation process in an FPW piezoelectric MEMS transducer for the controlled alignment of dry microparticle clusters at the microscale starting from a liquid droplet with microparticles dispersed therein. This article is organized as follows: working principle (Section II), design and fabrication of the MEMS transducer (Section III), 2-D finite-element analysis (Section IV), experimental results (Section V), and conclusion (Section VI).

II. Working Principle

The possibility of achieving aligned clusters of microparticles after complete evaporation of a liquid droplet into which they are initially dispersed has been explored by designing a dedicated piezoelectric MEMS transducer. Water has been used as the liquid in this study. The schematic top and

TABLE I
GEOMETRICAL AND MATERIAL PROPERTIES OF THE SI AND ALN LAYERS

Parameter	Description	Value
Silicon (Si)		
E_{Si}	Young's modulus	160 GPa
η_{Si}	Poisson's ratio	0.27
ρ_{Si}	Mass density	2329 kg/m^3
t_{Si}	Thickness	10 ± 1 µm
Aluminum nitride (AlN)		
E_{AlN}	Young's modulus	308 GPa
η_{AlN}	Poisson's ratio	0.24
ρ_{AlN}	Mass density	3250 kg/m^3
t_{AlN}	Thickness	0.5 µm

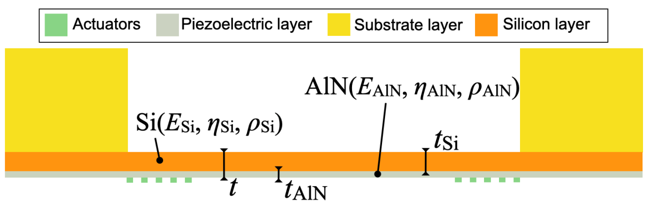

Fig. 3. Cross-sectional view of the MEMS transducer.

bottom views of the proposed MEMS transducer are shown in Fig. 1(a) and (b), respectively.

A squared cavity etched out in a silicon (Si) substrate is bounded by a composite diaphragm made of a stack of Si and piezoelectric layers. The composite diaphragm can be electrically actuated by means of metal interdigital transducers (IDTs) composed of interleaved comb-shaped electrodes with equally spaced fingers with pitch p. The liquid droplet is deposited on the substrate face of the diaphragm and used as a vehicle containing dispersed microparticles, as illustrated in Fig. 2(a). By applying sinusoidal excitation voltages between the fingers of the IDTs, a deformation of the piezoelectric layer is induced, which produces mechanical vibrations in the diaphragm in the form of Lamb plate waves. Specifically, by properly driving two opposed IDTs disposed symmetrically with respect to the device center, the first antisymmetric vibration mode (A_0) has been excited to generate standing FPWs in the diaphragm. The acoustic waves interact with the droplet transferring energy into the liquid in the form of compressional acoustic waves, as schematically shown in Fig. 2(b). The waves are attenuated in the liquid, thus forming a pressure gradient that initiates a flow inside the droplet, i.e., the acoustic stream flow (ASF) [30]. Due to evaporation, the contact angle θ_c between the diaphragm and the line tangent to the edge of the water droplet is progressively reduced [31] to θ_c', as shown in Fig. 2(c). With reducing θ_c, the pressure gradient lowers and the velocity and intensity of the ASF decrease in turn [32]. After complete evaporation, the electrical excitation is turned off and clusters of microparticles are expected to remain adhered to the diaphragm surface following a regular pattern with gap set by the acoustic wavelength [33], as shown in Fig. 2(d).

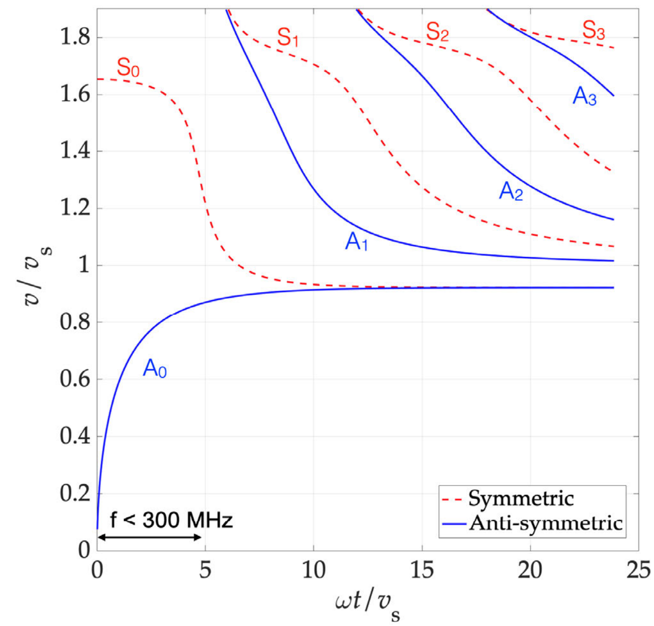

Fig. 4. Dispersion curves for Lamb waves propagating in the unbounded Si/AlN composite diaphragm.

III. DESIGN AND FABRICATION OF THE MEMS TRANSDUCER

The transducer has been designed and fabricated by using the piezoelectric multiuser MEMS process (PiezoMUMPs) made available by MEMSCAP, Crolles Cedex, France [34]. Material properties of the doped Si and aluminum nitride (AlN) piezoelectric layers that compose the diaphragm are shown in Table I. The design has been carried out considering the acoustic-fluidic coupling between the composite diaphragm and water by analyzing the symmetric (Sn) and antisymmetric (An) modes of plate waves [23]. The Young's modulus E, Poisson's ratio η, and mass density ρ of the Si/AlN composite diaphragm can be estimated as [35]

$$E = \frac{E_{Si}t_{Si} + E_{AlN}t_{AlN}}{t} \quad (1)$$

$$\eta = \frac{\eta_{Si}t_{Si} + \eta_{AlN}t_{AlN}}{t} \quad (2)$$

and

$$\rho = \frac{\rho_{Si}t_{Si} + \rho_{AlN}t_{AlN}}{t} \quad (3)$$

where $t = t_{Si} + t_{AlN}$ is the overall diaphragm thickness, as shown in Fig. 3, and subscripts Si and AlN refer to Si and piezoelectric layers, respectively. With the parameter values of Table I, it results $E = 167$ GPa, $\eta = 0.268$, and $\rho = 2373$ kg/m^3. Fig. 4 shows the computed dispersion curves of the Lamb waves for the composite unbounded Si/AlN two-layer diaphragm.

Specifically, the phase velocity v is plotted as a function of the product of angular frequency ω and thickness t. Both quantities are normalized to the phase velocity v_s of shear

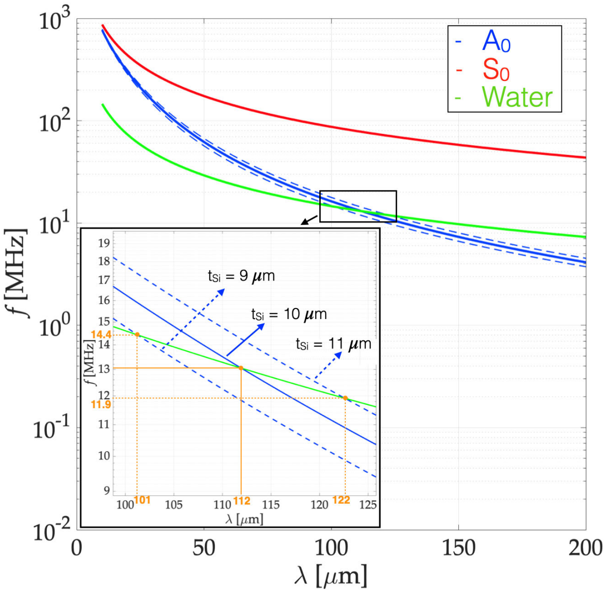

Fig. 5. Numerical analysis of frequency-to-wavelength relationships for the A_0 (blue curve) and S_0 (red curve) modes in the composite diaphragm and for the acoustic wave in water (green curve). Variations from the nominal curve, due to the fabrication tolerances, are shown in the inset (dashed curves).

waves in the Si/AlN bulk material of the diaphragm given by [36]

$$v_s = \sqrt{\frac{E}{2\rho(1+\eta)}} \tag{4}$$

which results equal to 5267 m/s. For the device under consideration, the symmetric S_0 and antisymmetric A_0 modes, related, respectively, to extensional and flexural waves [37], are the only two modes allowed for excitation frequencies lower than about 300 MHz. As the frequency increases, higher order plate modes arise while the phase velocities of S_0 and A_0 modes asymptotically converge to the velocity of the Rayleigh wave that is about $0.92v_s$ [38]. The frequencies f_{A0} and f_{S0} for the A_0 antisymmetric and S_0 symmetric modes can be expressed as [35], [39]

$$f_{A0} = \frac{2\pi t}{\lambda^2}\sqrt{\frac{E}{12(1-\eta^2)\rho}}\frac{1}{\sqrt{\frac{\pi^2 t^2}{3\lambda^2}+1}} \tag{5}$$

and

$$f_{S0} = \frac{1}{\lambda}\sqrt{\frac{E}{(1-\eta^2)\rho}}. \tag{6}$$

By employing (1)–(3), (5), (6), and the material parameters of Table I, a numerical analysis of the frequency-to-wavelength relationship of S_0 and A_0 modes has been carried out. The results are shown in Fig. 5, which also includes the frequency-to-wavelength relationship of acoustic waves in water given by

$$f_w = \frac{c_w}{\lambda} \tag{7}$$

where c_w is the sound speed in water of about 1460 m/s [40]. It can be observed that the A_0 mode intersects (7) at the frequency of 13 MHz where the wavelengths of the A_0 mode in the diaphragm and the longitudinal wave in water are equal. Blue dashed curves detail the f–λ relationship of the A_0 mode considering the manufacturing tolerances in the Si layer thickness.

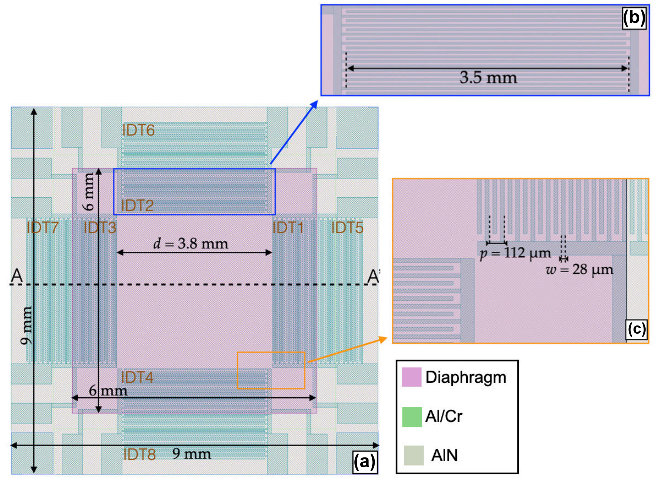

Fig. 6. (a) Bottom-view image of the proposed piezoelectric MEMS and (b) and (c) enlarged views of the IDTs taken from the GDS file.

Specifically, given the Si thickness $t_{Si} = 10 \pm 1$ μm, the intersection can be expected in the range $\lambda \approx 112 \pm 11$ μm and $f \approx 13 \pm 1.4$ MHz, as illustrated in the inset of Fig. 5. Therefore, the pitch p of the IDTs has been dimensioned to equal the nominal $\lambda = 112$ μm. More generally than the scope of this work, the device has been designed as a multipurpose piezoelectric MEMS platform that can be exploited to explore different applications [41], [42], [43].

The graphic design system (GDS) file displayed in Fig. 6(a) shows the bottom view of the device that includes eight IDTs placed at the inner and outer edges of the diaphragm symmetrically with respect to its center. Each IDT is composed of two interleaved comb-shaped arrays of 20 equally spaced fingers with an aperture of 3.5 mm to adequately couple the droplet with the generated 1-D acoustic field pattern and a width w of 28 μm, as visible in Fig. 6(b) and (c), respectively.

The silicon dioxide (SiO_2) and Si substrate layers have a thickness of 1 ± 0.05 and 400 ± 5 μm, respectively. The IDTs are made by a metal stack of 20 nm of chrome (Cr) and 1 μm of aluminum (Al). These values are defined by the fabrication process steps [34]. The top and bottom views of the fabricated piezoelectric MEMS transducer are shown in Fig. 7(a) and (b), respectively. Electrical terminal pads are provided for each IDT, as shown in Fig. 7(c). To induce standing FPWs in the diaphragm generating 1-D acoustic field pattern, the configuration of Fig. 8 has been adopted where only IDT1 and IDT3 are used, while the remaining IDTs included in the transducer are irrelevant for the present scope. A sinusoidal excitation voltage $v_{exc}(t)$ with peak amplitude A_{exc} and tunable frequency f_{exc} has been applied between the fingers of both IDT1 and IDT3, which are located symmetrically with respect to the diaphragm center [44].

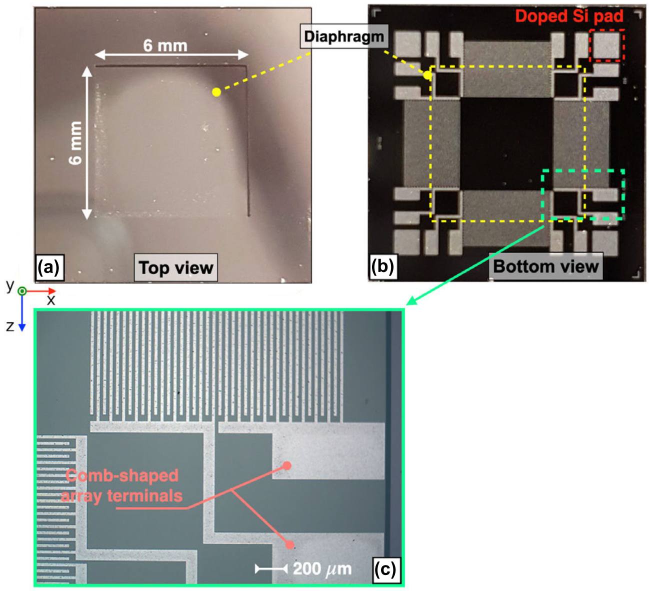

Fig. 7. (a) Top and (b) bottom views of the fabricated piezoelectric MEMS transducer. (c) Enlarged view of the terminal pads of the comb-shaped IDTs.

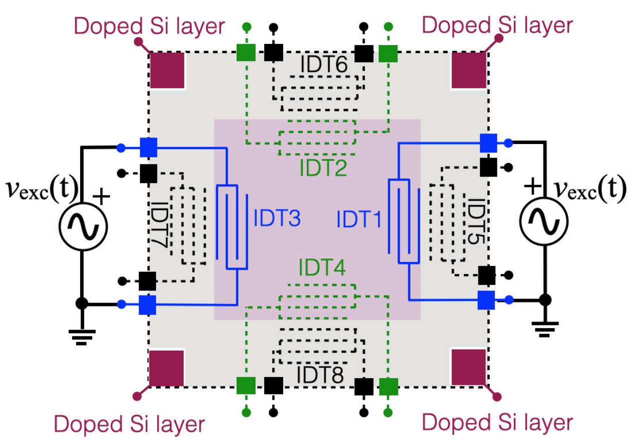

Fig. 8. Simplified schematic view of the piezoelectric MEMS transducer configured to achieve 1-D acoustic field pattern.

IV. 2-D Finite-Element Analysis

The electromechanical behavior of the piezoelectric MEMS transducer, described in Section II, has been investigated by means of 2-D finite-element modeling in COMSOL Multiphysics.[1]

The developed 2-D geometry is illustrated in Fig. 9(a) while Fig. 9(b) shows an enlarged view of the structural layers that have been considered in the model.

The nominal dimensions have been used, neglecting tolerances. Since the Al thickness is 50 times higher than the Cr thickness, only Al has been included in the model as the metal layer. SiO_2 and ⟨100⟩ Si have been used as the oxide layer and the substrate and Si layer materials, respectively. For the AlN layer, the piezoelectric coefficients $d_{31} = -2.78$ pC/N and $d_{33} = 6.5$ pC/N have been specified [45]. A generalized plane strain approximation has been assumed for the 2-D analysis.

[1]Registered trademark.

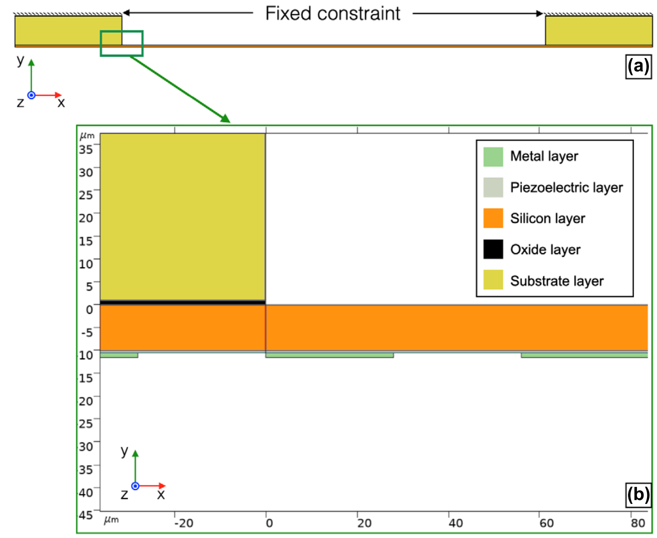

Fig. 9. (a) View of the 2-D model adopted for the proposed piezoelectric MEMS. (b) Enlarged view of the layers included in the simulation.

The piezoelectric effect has been simulated by including the piezoelectric multiphysics combining the solid mechanics with the electrostatics physics. Regarding the solid mechanics physics, a fixed constraint has been imposed to the top surface of the substrate while gravity constraint has been considered for the whole volume. To investigate the feasibility to induce standing waves in the composite diaphragm, an isotropic damping with a loss factor of 0.004 has also been considered and applied to the whole structure [46].

Dielectric losses and strain-charge constitutive relations have been specified for the piezoelectric layer including the AlN material properties, and a charge conservation boundary condition has been applied to the AlN layer in the electrostatics physics. Electrical domain constraints have been specified to the IDT fingers by alternating voltage and ground terminals. A floating potential group has been applied to the Si surface in contact with the AlN layer to take into account the high doping concentration and model a conductive electrode.

To identify the presence of standing FPWs and the position of pressure nodes, a time-domain simulation analysis has been performed by setting for the voltage of the IDTs a sinusoidal excitation $v_{exc}(t)$ with peak amplitude A_{exc} of 10 V and nominal frequency f_{exc} of 13 MHz as estimated in Section II. The obtained simulation results for the y-axis displacement are shown, not to scale, for the left and right sides of the diaphragm in Fig. 10(a) and (b), respectively. A standing flexural wave is induced with a maximum y-axis displacement of 0.45 nm and with pressure nodes evenly spaced by 56 μm, i.e., half the wavelength, in good agreement with the theoretical predictions of Section II.

V. Experimental Results

The electronic driving configuration adopted for experimental tests is shown in Fig. 11. By means of a two-channel waveform generator (Keysight 33522A), two sinusoidal signals $v_{s0}(t)$ and $v_{s1}(t)$ with the same peak-to-peak amplitude of 10 V

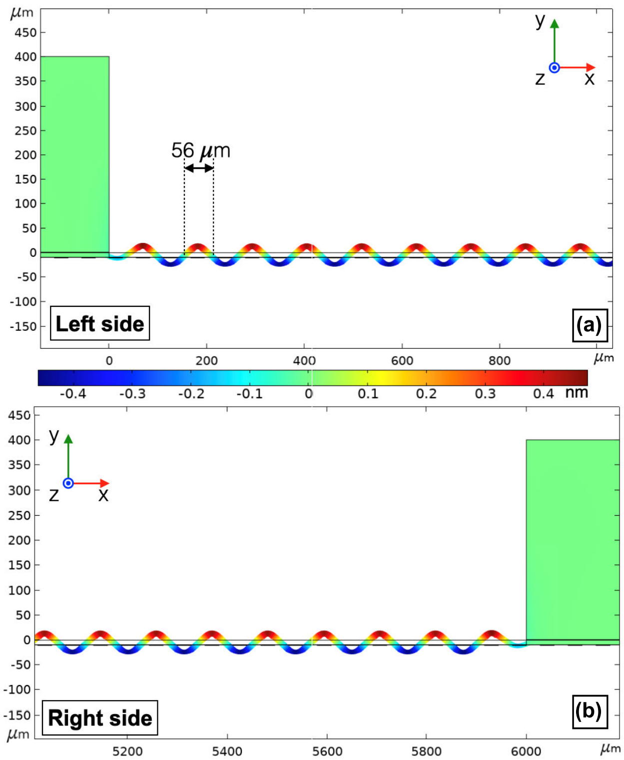

Fig. 10. Simulated y-axis displacement (not to scale) of the: (a) left and (b) right sides of the MEMS diaphragm under sinusoidal voltage excitation at a frequency of 13 MHz.

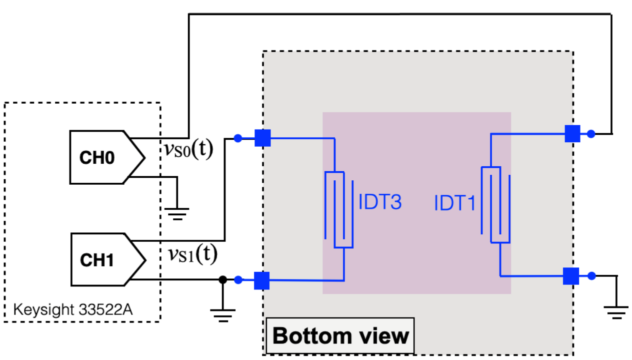

Fig. 11. Electrical configuration employed to generate deposits of aligned microparticles after evaporation of a water droplet.

and zero relative phase shift have been fed to IDT1 and IDT3 to drive the piezoelectric MEMS diaphragm at up to 15 MHz. The adopted experimental setup is shown in Fig. 12(a). A dedicated printed circuit board (PCB) hosts the MEMS transducer as visible in Fig. 12(b) and (c). A droplet of tap water with an approximate radius of 850 μm has been placed on the substrate face of the diaphragm as shown in the microscope (Motic PSM-1000) image of Fig. 13(a). As described in Section II, the droplet has been used as a vehicle to align microparticles, which are dissolved therein by exploiting evaporation at room temperature. Sinusoidal excitation voltages have been applied between the fingers of the IDTs located symmetrically with respect to the diaphragm center. This induces a deformation of the piezoelectric layer, which produces mechanical vibrations in the diaphragm in

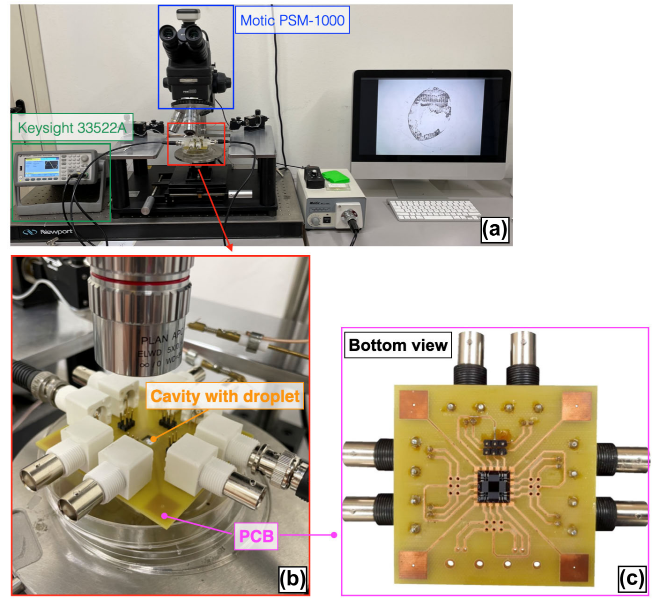

Fig. 12. (a) Experimental setup. (b) Top and (c) bottom views of the dedicated PCB hosting the piezoelectric MEMS device.

the form of Lamb plate waves, thus generating 1-D acoustic field pattern. The frequency of both the excitation signals $v_{s0}(t)$ and $v_{s1}(t)$ has been finely tuned until ripples into the water droplet were clearly visible from light reflections. This experimental approach allows to accurately adjust to the target condition. Such condition has been reached at the excitation frequency $f_{exc} = 12.5$ MHz, which lays in the 13 ± 1.4 MHz range theoretically predicted in Section II, corresponding to the situation where the wavelengths of the A_0 mode in the composite diaphragm and the longitudinal wave in water are equal. The driving sinusoidal signals $v_{s0}(t)$ and $v_{s1}(t)$ have then been maintained at such excitation frequency for the entire evaporation process, which took approximately 4 min.

An intermediate evaporation step showing the progressive reduction of the droplet volume is captured in Fig. 13(b). In Fig. 13(c), showing a subsequent image taken before the complete evaporation of the droplet, the 1-D acoustic field pattern can be clearly seen in the form of aligned ripples. This captured frame shows that by reducing the droplet volume and thus the contact angle, the pressure gradient induced by acoustic actuation lowers and the velocity and intensity of the ASF decrease in turn. This makes the acoustic radiation force generated by the 1-D acoustic field prevailing over the ASF, thus steering, agglomerating, and trapping microparticles and minerals dissolved in the tap water droplet at the nearest standing-wave node. After complete evaporation has occurred, clusters remain deposited on the diaphragm along a regular pattern with a gap of 56 μm, as shown in Fig. 13(d). The achieved gap is in accordance with theoretical predictions and finite element method (FEM) simulations since it corresponds to half the acoustic wavelength, i.e., where the standing-wave nodes are located [47]. The obtained experimental results confirm the feasibility to align clusters of microparticles in a drying water droplet by employing standing FPWs generated by a piezoelectric MEMS transducer.

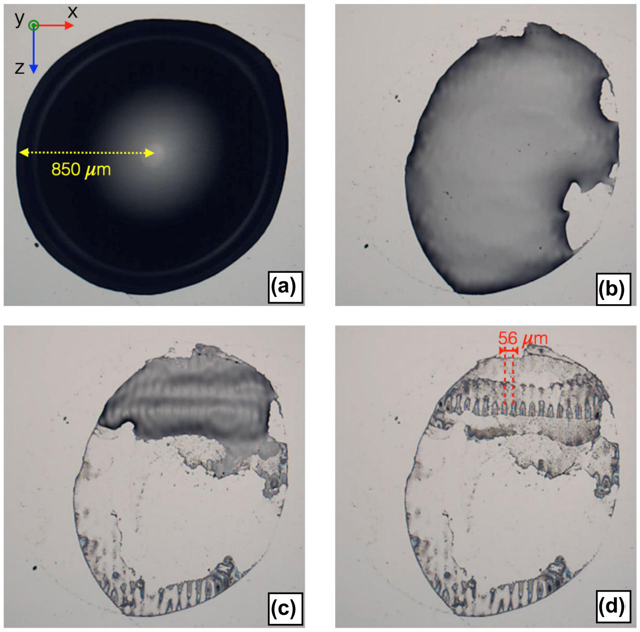

Fig. 13. Evaporation process steps of a tap water droplet deposited on the membrane of the piezoelectric MEMS device: (a) water droplet deposition; (b) intermediate evaporation step; (c) 1-D acoustic field pattern formation; and (d) particle alignment after complete evaporation.

VI. Conclusion

This work has presented a piezoelectric MEMS transducer able to achieve patterned clusters of microparticles after complete evaporation of a tap water droplet by employing standing FPWs. The acousto-fluidic coupling between the MEMS diaphragm and the liquid has been taken into account in the design of the device. The pitch of the IDTs has been set equal to the acoustic wavelength to generate at the same excitation frequency the A_0 flexural mode in the diaphragm and the longitudinal wave in the water droplet. The possibility to induce standing FPWs in the diaphragm has been investigated through a time-domain FEM analysis in COMSOL Multiphysics. A droplet with a radius of 850 μm of tap water has been deposited on the diaphragm and let dry at room temperature while tuning the frequency of the excitation sinusoidal signals applied to two opposed IDTs, until ripples were clearly visible from light reflections. This condition has been reached at the excitation frequency of 12.5 MHz, in good agreement with theoretical expectations and simulations. After complete water evaporation, the microparticles initially dispersed in the droplet have been arranged in dry clusters regularly spaced on the diaphragm with a pitch of half the acoustic wavelength, demonstrating that the proposed MEMS device is suitable for microassembly processes. The achieved results validate the possibility of innovatively combine the noncontact and noninvasive attributes of a flow-field-based approach with the label-free property of the evaporation process in a piezoelectric MEMS transducer. This can pave the way to the enhancement of assembly control of microparticles or biological cells in lab-on-chip applications and the development of novel diagnostic microtools for biomedical applications.

References

[1] A. B. Kotlyar, N. Borovok, T. Molotsky, H. Cohen, E. Shapir, and D. Porath, "Long, monomolecular guanine-based nanowires," *Adv. Mater.*, vol. 17, no. 15, pp. 1901–1905, Aug. 2005, doi: 10.1002/adma.200401997.

[2] D. Pavc et al., "Understanding self-assembly at molecular level enables controlled design of DNA G-wires of different properties," *Nature Commun.*, vol. 13, no. 1, p. 1062, Feb. 2022, doi: 10.1038/s41467-022-28726-6.

[3] H. Ko and V. V. Tsukruk, "Liquid-crystalline processing of highly oriented carbon nanotube arrays for thin-film transistors," *Nano Lett.*, vol. 6, no. 7, pp. 1443–1448, Jul. 2006, doi: 10.1021/nl060608r.

[4] B. Liu and E. S. Aydil, "Growth of oriented single-crystalline rutile TiO_2 nanorods on transparent conducting substrates for dye-sensitized solar cells," *J. Amer. Chem. Soc.*, vol. 131, no. 11, pp. 3985–3990, Mar. 2009, doi: 10.1021/ja8078972.

[5] N. Lavielle, A. Hébraud, L. Thöny-Meyer, R. M. Rossi, and G. Schlatter, "3D composite assemblies of microparticles and nanofibers for tailored wettability and controlled drug delivery," *Macromolecular Mater. Eng.*, vol. 302, no. 8, Aug. 2017, Art. no. 1600458, doi: 10.1002/mame.201600458.

[6] A. Testa et al., "Sustained enzymatic activity and flow in crowded protein droplets," *Nature Commun.*, vol. 12, no. 1, p. 6293, Nov. 2021, doi: 10.1038/s41467-021-26532-0.

[7] M. Grzelczak, J. Vermant, E. M. Furst, and L. M. Liz-Marzán, "Directed self-assembly of nanoparticles," *ACS Nano*, vol. 4, no. 7, pp. 3591–3605, Jul. 2010, doi: 10.1021/nn100869j.

[8] K. J. M. Bishop, C. E. Wilmer, S. Soh, and B. A. Grzybowski, "Nanoscale forces and their uses in self-assembly," *Small*, vol. 5, no. 14, pp. 1600–1630, Jul. 2009, doi: 10.1002/smll.200900358.

[9] R. W. O'Brien and L. R. White, "Electrophoretic mobility of a spherical colloidal particle," *J. Chem. Soc., Faraday Trans.*, vol. 74, pp. 1607–1626, Jan. 1978, doi: 10.1039/f29787401607.

[10] S. H. Lee and C. M. Liddell, "Anisotropic magnetic colloids: A strategy to form complex structures using nonspherical building blocks," *Small*, vol. 5, no. 17, pp. 1957–1962, Sep. 2009, doi: 10.1002/smll.200900135.

[11] S. Kanafusa, U. Maspero, M. A. Petersen, and F. G. Galindo, "Influence of pulsed electric field-assisted dehydration on the volatile compounds of basil leaves," *Innov. Food Sci. Emerg. Technol.*, vol. 77, May 2022, Art. no. 102979, doi: 10.1016/j.ifset.2022.102979.

[12] B. J. Ackerson, "Shear induced order and shear processing of model hard sphere suspensions," *J. Rheol.*, vol. 34, no. 4, pp. 553–590, May 1990, doi: 10.1122/1.550096.

[13] M. Serzanti et al., "Arrangement of live human cells through acoustic waves generated by piezoelectric actuators for tissue engineering applications," *Appl. Sci.*, vol. 10, no. 10, p. 3477, May 2020, doi: 10.3390/app10103477.

[14] J. Qian, J. Ren, W. Huang, R. H. W. Lam, and J. E.-Y. Lee, "Acoustically driven manipulation of microparticles and cells on a detachable surface micromachined silicon chip," *IEEE Sensors J.*, vol. 21, no. 10, pp. 11999–12008, May 2021, doi: 10.1109/JSEN.2021.3065694.

[15] M. A. Burguillos et al., "Microchannel acoustophoresis does not impact survival or function of microglia, leukocytes or tumor cells," *PLoS ONE*, vol. 8, no. 5, May 2013, Art. no. e64233, doi: 10.1371/journal.pone.0064233.

[16] X. Ding, J. Shi, S.-C.-S. Lin, S. Yazdi, B. Kiraly, and T. J. Huang, "Tunable patterning of microparticles and cells using standing surface acoustic waves," *Lab Chip*, vol. 12, no. 14, pp. 2491–2497, 2012, doi: 10.1039/c2lc21021e.

[17] M. Wu, A. Ozcelik, J. Rufo, Z. Wang, R. Fang, and T. J. Huang, "Acoustofluidic separation of cells and particles," *Microsyst. Nanoeng.*, vol. 5, no. 1, p. 32, Jun. 2019, doi: 10.1038/s41378-019-0064-3.

[18] L. Malik, A. Nath, S. Nandy, T. Laurell, and A. K. Sen, "Acoustic particle trapping driven by axial primary radiation force in shaped traps," *Phys. Rev. E, Stat. Phys. Plasmas Fluids Relat. Interdiscip. Top.*, vol. 105, no. 3, Mar. 2022, Art. no. 035103, doi: 10.1103/physreve.105.035103.

[19] F. Guo et al., "Three-dimensional manipulation of single cells using surface acoustic waves," *Proc. Nat. Acad. Sci. USA*, vol. 113, no. 6, pp. 1522–1527, Feb. 2016, doi: 10.1073/pnas.1524813113.

[20] P. Reichert, D. Deshmukh, L. Lebovitz, and J. Dual, "Thin film piezoelectrics for bulk acoustic wave (BAW) acoustophoresis," *Lab Chip*, vol. 18, no. 23, pp. 3655–3667, 2018, doi: 10.1039/c8lc00833g.

[21] R. M. Moroney, R. M. White, and R. T. Howe, "Microtransport induced by ultrasonic Lamb waves," *Appl. Phys. Lett.*, vol. 59, no. 7, pp. 774–776, Aug. 1991, doi: 10.1063/1.105339.

[22] W. Wang et al., "Laser-induced surface acoustic wave sensing-based malaria parasite detection and analysis," *IEEE Trans. Instrum. Meas.*, vol. 71, pp. 1–9, 2022, doi: 10.1109/TIM.2021.3124841.

[23] V. Ferrari and R. Lucklum, "Overview of acoustic-wave microsensors," in *Piezoelectric Transducers and Applications*, A. A. Vives, Ed. Berlin, Germany: Springer, 2004, doi: 10.1007/978-3-662-05361-4_2.

[24] F. Guo et al., "Controlling cell–cell interactions using surface acoustic waves," *Proc. Nat. Acad. Sci. USA*, vol. 112, no. 1, pp. 43–48, Jan. 2015, doi: 10.1073/pnas.1422068112.

[25] Y. Zhao, G. Cavallaro, and Y. Lvov, "Orientation of charged clay nanotubes in evaporating droplet meniscus," *J. Colloid Interface Sci.*, vol. 440, pp. 68–77, Feb. 2015, doi: 10.1016/j.jcis.2014.10.050.

[26] R. Bhardwaj, X. Fang, and D. Attinger, "Pattern formation during the evaporation of a colloidal nanoliter drop: A numerical and experimental study," *New J. Phys.*, vol. 11, no. 7, Jul. 2009, Art. no. 075020, doi: 10.1088/1367-2630/11/7/075020.

[27] T. A. Yakhno et al., "Drying drops of biological liquids: Dynamics of the optical and mechanical properties. Application in rapid medical diagnostics," *Proc. SPIE*, vol. 5692, pp. 188–198, Apr. 2005, doi: 10.1117/12.591556.

[28] Y. Zhou, J. Hu, and S. Bhuyan, "Manipulations of silver nanowires in a droplet on a low-frequency ultrasonic stage," *IEEE Trans. Ultrason., Ferroelectr., Freq. Control*, vol. 60, no. 3, pp. 622–629, Mar. 2013, doi: 10.1109/TUFFC.2013.2604.

[29] Y. Zhu et al., "Evaporation-Induced vertical alignment enabling directional ion transport in a 2D-nanosheet-based battery electrode," *Adv. Mater.*, vol. 32, no. 10, Mar. 2020, Art. no. 1907941, doi: 10.1002/adma.201907941.

[30] G. Destgeer, B. Ha, J. Park, and H. J. Sung, "Lamb wave-based acoustic radiation force-driven particle ring formation inside a sessile droplet," *Anal. Chem.*, vol. 88, no. 7, pp. 3976–3981, Apr. 2016, doi: 10.1021/acs.analchem.6b00213.

[31] G. Destgeer, J. H. Jung, J. Park, H. Ahmed, and H. J. Sung, "Particle separation inside a sessile droplet with variable contact angle using surface acoustic waves," *Anal. Chem.*, vol. 89, no. 1, pp. 736–744, Jan. 2017, doi: 10.1021/acs.analchem.6b03314.

[32] J. Nam, W. S. Jang, J. Kim, H. Lee, and C. S. Lim, "Lamb wave-based molecular diagnosis using DNA hydrogel formation by rolling circle amplification (RCA) process," *Biosensors Bioelectron.*, vol. 142, Oct. 2019, Art. no. 111496, doi: 10.1016/j.bios.2019.111496.

[33] D. J. Collins, B. Morahan, J. Garcia-Bustos, C. Doerig, M. Plebanski, and A. Neild, "Two-dimensional single-cell patterning with one cell per well driven by surface acoustic waves," *Nature Commun.*, vol. 6, no. 1, p. 8686, Nov. 2015, doi: 10.1038/ncomms9686.

[34] A. Cowen, G. Hames, K. Glukh, and B. Hardy, *PiezoMUMPs Design Handbook*. Durham, NC, USA: MEMSCAP, 2014.

[35] Y. Liu et al., "Flexible and bendable acoustofluidics based on ZnO film coated aluminium foil," *Sens. Actuators B, Chem.*, vol. 221, pp. 230–235, Dec. 2015, doi: 10.1016/j.snb.2015.06.083.

[36] I. Z. Nenadic, M. W. Urban, M. Bernal, and J. F. Greenleaf, "Phase velocities and attenuations of shear, Lamb, and Rayleigh waves in plate-like tissues submerged in a fluid (L)," *J. Actuators Soc. Amer.*, vol. 130, no. 6, pp. 3549–3552, Dec. 2011, doi: 10.1121/1.3654029.

[37] S. Braun, D. Ewins, and S. S. Rao, "Wave propagation," in *Encyclopedia of Vibration*. London, U.K.: Academic Press, 2002, pp. 1551–1564, doi: 10.1006/rwvb.2001.

[38] M. Hamidullah, C. Élie-Caille, and T. Leblois, "Higher-order Lamb waves with quasi-zero surface displacement components on a GaAs piezoelectric plate," *J. Phys. D, Appl. Phys.*, vol. 55, no. 9, Mar. 2022, Art. no. 094003, doi: 10.1088/1361-6463/ac39c5.

[39] M. Demori, M. Baù, M. Ferrari, S. Basrour, L. Rufer, and V. Ferrari, "MEMS device with piezoelectric actuators for driving mechanical vortexes in aqueous solution drop," in *Proc. 20th Int. Conf. Solid-State Sensors, Actuat. Microsystems Eurosensors*, Jun. 2019, pp. 2318–2321, doi: 10.1109/TRANSDUCERS.2019.8808791.

[40] A. G. Athanassiadis and D. P. Hart, "Broadband leaky Lamb waves excited by optical breakdown in water," *J. Acoust. Soc. Amer.*, vol. 146, no. 2, pp. 885–892, Aug. 2019, doi: 10.1121/1.5120182.

[41] A. Nastro, M. Baù, M. Ferrari, and V. Ferrari, "Piezoelectric MEMS for sensors, actuators and energy harvesting," in *Sensors and Microsystems*. Cham, Switzerland: Springer, 2021, doi: 10.1007/978-3-031-08136-1_41.

[42] A. Nastro, M. Ferrari, L. Rufer, S. Basrour, and V. Ferrari, "Piezoelectric MEMS acoustic transducer with electrically-tunable resonant frequency," *Micromachines*, vol. 13, no. 1, p. 96, Jan. 2022, doi: 10.3390/mi13010096.

[43] A. Nastro, L. Rufer, M. Ferrari, S. Basrour, and V. Ferrari, "Piezoelectric micromachined acoustic transducer with electrically-tunable resonant frequency," in *Proc. 20th Int. Conf. Solid-State Sensors, Actuat. Microsystems Eurosensors*, Jun. 2019, pp. 1905–1908, doi: 10.1109/TRANSDUCERS.2019.8808488.

[44] Y. Xie et al., "Acoustic cell separation based on density and mechanical properties," *J. Biomechanical Eng.*, vol. 142, no. 3, Mar. 2020, Art. no. 031005, doi: 10.1115/1.4046180.

[45] M. Kabir, H. Kazari, and D. Ozevin, "Piezoelectric MEMS acoustic emission sensors," *Sens. Actuators A, Phys.*, vol. 279, pp. 53–64, Aug. 2018, doi: 10.1016/j.sna.2018.05.044.

[46] D. W. Branch, K. E. Wojciechowski, and R. H. Olsson, "Elucidating the origin of spurious modes in aluminum nitride microresonators using a 2-D finite-element model," *IEEE Trans. Ultrason., Ferroelectr., Freq. Control*, vol. 61, no. 5, pp. 729–738, May 2014, doi: 10.1109/TUFFC.2014.2965.

[47] A. Nastro, M. Baù, M. Ferrari, L. Rufer, S. Basrour, and V. Ferrari, "Cell alignment in aqueous solution employing a flexural plate wave piezoelectric MEMS transducer," *IEEE Access*, vol. 11, pp. 130755–130762, 2023, doi: 10.1109/ACCESS.2023.3333694.

Alessandro Nastro (Member, IEEE) was born in Romano di Lombardia, Italy, in 1991. He received the master's (cum laude) degree in electronics engineering and the Europaeus Ph.D. degree in information engineering from the University of Brescia, Brescia, Italy, in 2016 and 2020, respectively.

Since 2019, he has been a Research Fellow of Electronics, and since May 2022, he has been an Assistant Professor with the Department of Information Engineering, University of Brescia. He has coauthored more than 20 publications in international peer-reviewed journals and international and national conference proceedings. His research activity deals with the development of electronic techniques and circuits coupled to MEMS for static and dynamic micromechanical sensing and actuation.

Dr. Nastro is a member of the Italian National Research Council (CNR).

Marco Baù (Member, IEEE) was born in Castiglione delle Stiviere, Italy, in 1981. He received the Laurea (cum laude) degree in electronic engineering and the Research Doctorate degree in electronic instrumentation from the University of Brescia, Brescia, Italy, in 2005 and 2009, respectively.

From 2009 to September 2018, he was a Research Assistant of Electronics, and since October 2018, he has been an Assistant Professor with the Department of Information Engineering, University of Brescia. His research activities deal with the investigation of techniques for the contactless interrogation of resonant and capacitive sensors for autonomous electronics devices, the design of MEMS sensors and the related front-end electronic circuits, and the investigation of principles and techniques for energy harvesting from vibrations adopting linear and nonlinear conversion techniques.

Marco Ferrari (Member, IEEE) was born in Brescia, Italy, in 1974. He received the Laurea degree in electronics engineering and the Research Doctorate degree in electronic instrumentation from the University of Brescia, Brescia, in 2002 and 2006, respectively.

He was an Assistant Professor from 2007 to 2015, an Associate Professor from 2015 to 2020, and since 2020, he has been a Full Professor of Electronics with the Department of Information Engineering, University of Brescia. He has coauthored more than 100 publications in international peer-reviewed journals and international conference proceedings, and a patent with industrial exploitation. His research activity deals with the energy conversion via the piezoelectric and thermoelectric effect for powering autonomous microsystems, sensors for physical and chemical quantities, signal-conditioning electronics, oscillators, frequency-output interface circuits, resonant microsensors, and MEMS.

Dr. Ferrari is also an Associate Member of the Italian National Research Council (CNR) and National Institute of Nuclear Physics (INFN).

Libor Rufer (Senior Member, IEEE) received the Engineer and Ph.D. degrees from Czech Technical University, Prague, Czechia, in 1974 and 1984, respectively.

Until 1993, he was with the Faculty of Electrical Engineering, Czech Technical University. Since 1994, he has been an Associate Professor and later a Senior Scientist with the University of Grenoble, Grenoble, France. In 1998, he joined the Microsystems Group, TIMA Laboratory, Grenoble. Since 2021, he has been with Advanced Design and Technology for MEMS (ADT MEMS), Grenoble. His expertise is mainly in MEMS-based sensors and actuators, electroacoustic and electromechanical transducers, and their applications in acoustics, ultrasonics, and energy harvesting. He participated in the number of French and European projects, and has authored more than 150 articles in refereed international journals and conferences.

Dr. Rufer is a committee member of competitive international conferences and a reviewer of the number of prestigious journals and conferences in the field of MEMS and acoustics.

Skandar Basrour (Member, IEEE) received the degree in physics and chemistry from the Ecole Normale Supeìrieure de Tunis, Tunis, Tunisia, in 1986, and the Ph.D. degree in microelectronics from the Universiteì Joseph Fourier, Grenoble, France, in 1990.

From 1992 to 2001, he was an Assistant Professor of Electronics and Microsystems with the Universiteì de Franche-Comteì, Besançon, France. He contributed to the development and the improvement of the X-ray and UV lithographie galvanoformung abformung – lithography, electroplating, and molding (LIGA), microfabrication techniques. Since 2001, he has been a Full Professor of Electronics and Microsystems with the Polytech School of Engineering, University of Grenoble Alpes, Grenoble. He was the Leader of the Micro and Nano Systems Group, TIMA Laboratory, Grenoble, for 12 years, where he has been a Co-Leader of the CDSI Group, since 2013, and has been the Deputy Director, since 2015. His research activities are focused on the design, fabrication, and characterization of high-Q microresonator and nanoresonator as a time reference. In recent years, he propelled the design of new micropower generators based on piezoelectric thin films (PiezoMEMS). More recently, he started working on acoustic devices, such as microphones for aeroacoustics metrology and tactile devices using ultrasound waves for haptic rendering.

Vittorio Ferrari (Senior Member, IEEE) received the Laurea (cum laude) degree in physics from the University of Milan, Milan, Italy, in 1988, and the Ph.D. degree in electronic instrumentation from the University of Brescia, Brescia, Italy, in 1993.

He has been a Full Professor of Electronics with the University of Brescia, since 2006. From 2016 to 2022, he was the Rectors's delegate for research quality management and postgraduate studies with the University of Brescia. He has authored or coauthored more than 250 publications in international peer-reviewed journals and conference proceedings, invited presentations, and book chapters, and holds seven patents. He and his group are active in research projects, with both academic and industrial participation, on piezoelectric transducers and resonant microsensors, energy harvesting for autonomous sensors, MEMS and microsystems, sensors with contactless interrogation, electronic interfaces for sensor signals, sensing systems for fluidics, and wearable devices.

Dr. Ferrari is currently an Associate Member of the Italian National Research Council (CNR) and National Institute of Nuclear Physics (INFN). He serves in international panels, conference committees, including IEEE UFFC-IUS Group 5, and boards in the field of sensors and electronic instrumentation. He was the Program Chair of the Eurosensors Conference 2014.

Open Access funding provided by 'Università degli Studi di Brescia' within the CRUI-CARE Agreement